Virology 432 (2012) 204–218

Contents lists available at SciVerse ScienceDirect

Virology

journal homepage: www.elsevier.com/locate/yviro

The influenza fingerprints: NS1 and M1 proteins contribute to specific host cell ultrastructure signatures upon infection by different influenza A viruses

Olivier Terrier [a,1], Vincent Moules [a,1], Coralie Carron [a], Gaëlle Cartet [a], Emilie Frobert [b], Matthieu Yver [a], Aurelien Traversier [a], Thorsten Wolff [c], Beatrice Riteau [d], Nadia Naffakh [e], Bruno Lina [b,d], Jean-Jacques Diaz [f], Manuel Rosa-Calatrava [a,*]

[a] Equipe VirCell, Laboratoire de Virologie et Pathologie Humaine, VirPath EMR 4610, Université de Lyon, Université Claude Bernard Lyon 1, Hospices Civils de Lyon, Faculté de médecine RTH Laennec, rue Guillaume Paradin, F-69008 Lyon, France
[b] Laboratoire de Virologie, Centre de Biologie et de Pathologie Est, Hospices Civils de Lyon, 59 boulevard Pinel, F-69677 Bron Cedex, Lyon, France
[c] Division of Influenza/Respiratory Viruses, Robert Koch Institute, Nordufer 20, D-13353 Berlin, Germany
[d] Laboratoire de Virologie et Pathologie Humaine, VirPath EMR 4610, Université de Lyon, Université Claude Bernard Lyon 1, Hospices Civils de Lyon, Faculté de médecine RTH Laennec, rue Guillaume Paradin, F-69008 Lyon, France
[e] Institut Pasteur, Unité de Génétique Moléculaire des Virus Respiratoires, URA CNRS 3015, EA302 Université Paris Diderot, Paris, France
[f] Centre de Recherche en Cancérologie de Lyon UMR Inserm 1052 CNRS 5286, Centre Léon Bérard, FNCLCC, F-69373 Lyon, France

ARTICLE INFO

Available online 6 July 2012

Keywords:
Influenza
Host cellular ultrastructure
Nucleolus
Infection fingerprints
NS1 and M1 viral proteins

ABSTRACT

Influenza A are nuclear replicating viruses which hijack host machineries in order to achieve optimal infection. Numerous functional virus–host interactions have now been characterized, but little information has been gathered concerning their link to the virally induced remodeling of the host cellular architecture. In this study, we infected cells with several human and avian influenza viruses and we have analyzed their ultrastructural modifications by using electron and confocal microscopy. We discovered that infections lead to a major and systematic disruption of nucleoli and the formation of a large number of diverse viral structures showing specificity that depended on the subtype origin and genomic composition of viruses. We identified NS1 and M1 proteins as the main actors in the remodeling of the host ultra-structure and our results suggest that each influenza A virus strain could be associated with a specific cellular fingerprint, possibly correlated to the functional properties of their viral components.

Introduction

Influenza A viruses are responsible for recurrent annual epidemics and constitute a major threat to public health with the potential to mutate into new pandemic subtypes, as was recently illustrated with the A(H1N1)pdm2009 (Neumann et al., 2009; Michaelis et al., 2009).

Influenza A virus genomes consist of eight RNA negative segments existing as ribonucleoprotein complexes (vRNP) (Palese and Shaw, 2007) and their replication cycle occurs within the nucleus of the host cells (for a review: Josset et al., 2008). Nuclear import of the viral genome is followed by an initial round of transcription driven by the viral polymerase (RNA-dependent RNA-polymerase, RdRp) for the production of early mRNA. Subsequently, RdRp initiates the replication of vRNA by elongating intermediate positive RNA (cRNA), which will constitute the matrix for the synthesis of numerous copies of new vRNA genome (Neumann et al., 2004). Despite the increasing number of available molecular data concerning the functional interplay between influenza A and cellular components (Nagata et al., 2008; Karlas et al., 2010; König et al., 2010) several "black boxes" still need to be explored to allow a more complete understanding of the fundamental biology of influenza viruses.

Several groups, including ours, have hypothesized that the dynamic and spatial architecture of the host nuclear compartment may contribute to the regulation of viral molecular mechanisms (Amorim and Digard, 2006; Lamond and Sleeman, 2003; Josset et al., 2008). In such a context, several specific virally induced nuclear structures were found to reflect viral activities such as replication, transcription or RNA splicing as well as trafficking for DNA viruses with a nuclear replication cycle (i.e. adenoviruses or herpesviruses). The formation of such structures is a characteristic of the viral hijacking of the host nuclear machinery (Hiscox, 2006). However, little is known about influenza-induced modifications of the host nuclear architecture (Josset et al., 2008).

* Corresponding author. Fax: +33 4 78 77 87 51.
E-mail address: manuel.rosa-calatrava@univ-lyon1.fr (M. Rosa-Calatrava).
[1] OT and VM have contributed equally to the present work.

0042-6822/$ - see front matter © 2012 Elsevier Inc. All rights reserved.
http://dx.doi.org/10.1016/j.virol.2012.05.019

Of the several electron microscopic investigations performed in the 1960s, 70s and 80s most were in non-human cellular models infected with a very limited number of influenza strains (A/Puerto Rico/8/34 (PR8) or A/WSN/33 (WSN)). These studies systematically showed modifications of nucleolar architecture and reported different types of virally induced structures, such as nuclear elongated tubular structures or cytoplasmic dense inclusion-like bodies (Anisimova et al., 1980; Anisimová et al., 1977; Kopp et al., 1968; Saito et al., 1970; Josset et al., 2008). However, no viral factors were characterized for their involvement in this host cell remodeling and the functional significance of these virally induced structures remains to be elucidated. Moreover, to our knowledge, none of the electron microscopic investigations were undertaken to systematically compare different influenza A strains for their ability to alter host cellular architecture.

The aim of this study was therefore to build on these original studies by scrutinizing more precisely the host cellular modifications induced by several different influenza A viruses. We had a particular focus on the nucleolar compartment and the alterations of which appear to be the most marked during infection (Josset et al., 2008). Using electron microscopy (EM) and confocal microscopy, we studied both human pulmonary epithelial cells (A549) and primary chicken embryonic fibroblasts (CEF) infected with different pandemic and epidemic human influenza strains and with low or highly pathogenic avian subtypes.

Altogether, our results reveal an unexpected subtype-specific heterogeneity in viral alterations of the host architecture and the formation of a large number of diversified structures that depend on the viral strain origin. Moreover, immunostaining experiments and the study of different recombinant viruses suggest, for the first time, that specific virally induced structures are dependent of the strain origin of NS1 and M1 proteins.

Results

In order to investigate the host cell ultrastructural modifications induced upon influenza infection, we first examined mock-infected human respiratory epithelial A549 cells to refer to as the normal ultrastructural morphology of these cells. As shown in Fig. 1, the regular architecture of the nucleus (Fig. 1, panel a) comprises a nucleoli (Nu) harboring several fibrillar centers (FC) surrounded by dense fibrillar components (DFC) and granular components (GC) (Fig. 1, panel a1). The A549 cells present a cytoplasmic morphology and organelle localization (Fig. 1, panel a2) that reflect well the expected polarized state of respiratory epithelial cells. The following results presented in this study are based on representative pictures of infected cells obtained in repeated experiments, as described in Materials and Methods.

A/Moscow/10/99 (H3N2) virus induces a major remodeling of host nuclear and nucleolar ultrastructures

Human cells (A549) were infected with A/Moscow/10/99 (H3N2) (MO) virus and observed by EM (Fig. 2A, panels a1–a4). Concomitantly, stages of infection were determined by confocal microscopy by immunostaining of nucleoprotein (NP), as presented in Fig. 2B.

The most striking observation was the extensive alteration of the nucleoli (Fig. 2A, panels a5–a8). This remodeling was characterized by a progressive disappearance of the constitutive FC and DFC, which was achieved by 10 hpi (Fig. 2A, panel a7). Concomitantly, numerous electron dense round-shaped bodies (indicated by stars) of increasing size were found accumulated throughout the nucleolar space leading to the spotty appearance of this compartment shown at high magnification in Fig. 2C (panel c1).

Furthermore, several rod-like structures were detected within the nucleoplasm later on in infection (Fig. 2A, panel a8, structures indicated by arrows). These structures, measuring 40–60 nm in diameter, were of various lengths and presented a regular dense striation perpendicular to the long axis with a seemingly central hole, as observed in longitudinal and transversal views, respectively (Fig. 2C, panels c2–c5). In cross section, they appeared to be formed by the regular close arrangement of striae of 9.8 ± 0.7 nm in diameter (mean°standard deviation, SD; n, number of independent measurements in different cross-sectional areas=20). In longitudinal sections, the inter-striae distance was found to be 8.4 ± 0.5 nm (mean $\pm$ SD; $n=25$).

In the cytoplasm, dense irregularly shaped materials were found accumulated in clusters (**Supplementary Fig. 1**), their number and size were growing as the infection progressed (data not shown). In favorable sections, these structures can be described as paracrystalline-like inclusions surrounded by numerous punctuated structures resembling to ribosomes (**Supplementary Fig. 1**, panels a2 and a3 and data not shown). It is interesting to note that similar structures were previously reported within WSN H1N1 infected cells (Kopp et al., 1968;

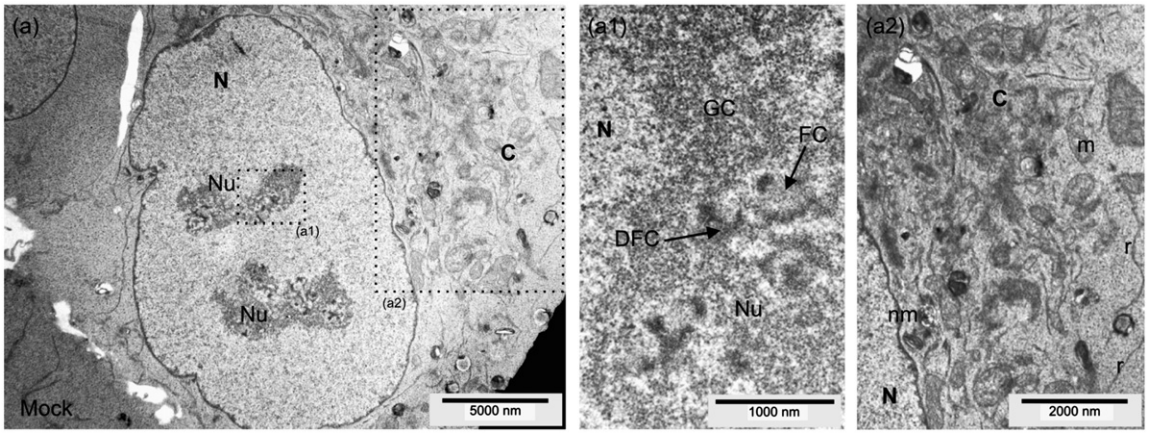

Fig. 1. Regular ultrastructure of A549 cells. Glutaraldehyde fixation and Epon embedding. Architectures of nucleus and cytoplasm of mock-infected A549 cells are observed in panel (a). Enlargement of frames shows nucleolar sub-domains (DFC, FC and GC) in (a1) and cytoplasmic morphology and organelles in (a2). C: cytoplasm; DFC: dense fibrillar component; FC: fibrillar center; GC: granular component; m: mitochondria; N: nucleus; nm: nuclear membrane; Nu: nucleolus. Scale bars are indicated.

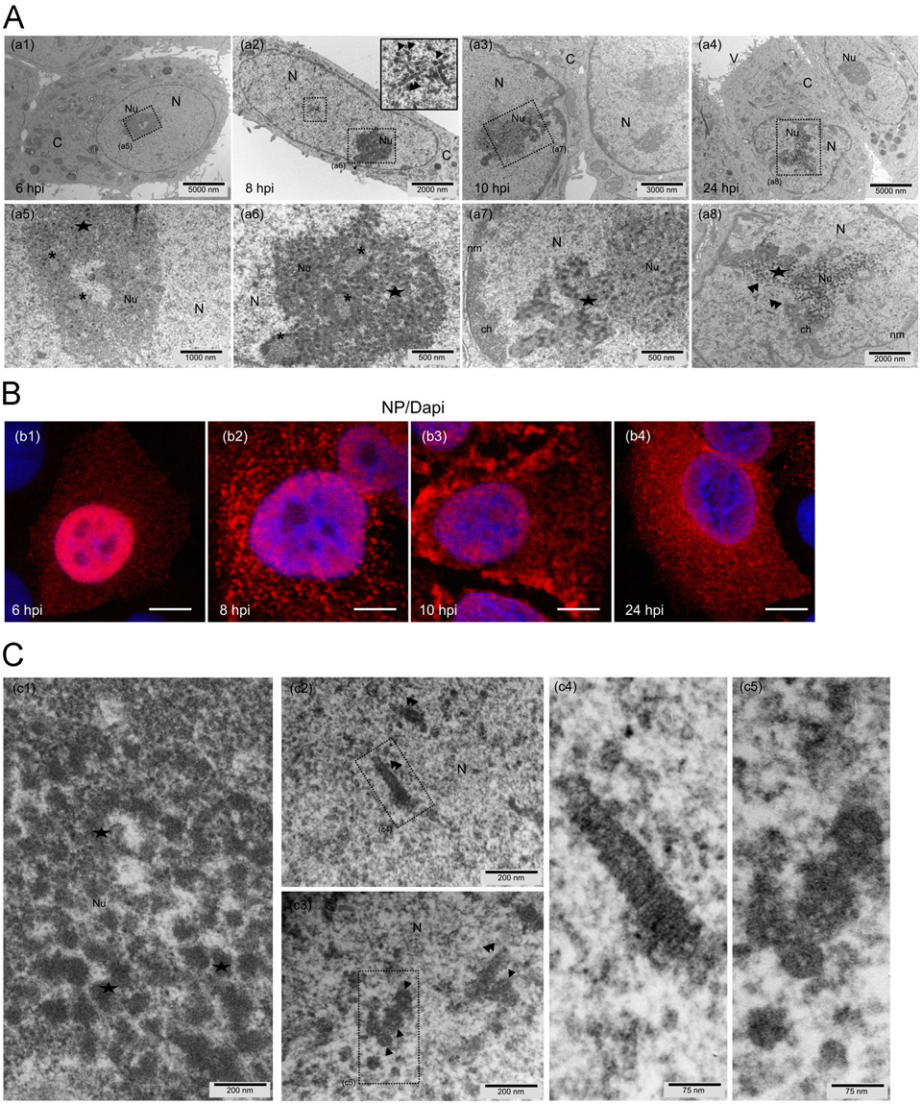

Fig. 2. Dynamic remodeling of the host nuclear and nucleolar ultrastructures during infection by MO virus. A. Glutaraldehyde fixation and Epon embedding. (a1–a4). General aspect of infected cells at several time points following infection (MOI 1). (a5–a8) Enlargements of frames show a strong remodeling of the nucleolar compartment characterized by the progressive disappearance of FC and DFC (asterisk) and the accumulation of increasingly numerous electron dense round-shaped bodies (stars). Several rod-like structures can be seen accumulated within the nucleoplasm late in infection (double arrowheads). Scale bars are indicated. B. NP immunostaining of infected A549 cells. At several time points post-infection, immunolabeling was performed with anti-NP (red) and appropriate secondary antibodies. Nuclei were stained with DAPI (blue). Panels (b1–b4) are the merged confocal images from each fluorochrome. Scale bars, 10 μm. C. Higher magnifications of the virally induced nucleolar remodeling (c1, stars). Transversal (arrowhead) and longitudinal (double arrowhead) views of the striated rod-like structures are observed in panels (c2, c4) and (c3, c5), respectively. Scale bars are indicated. C, cytoplasm; ch, chromatin; DFC, dense fibrillar component; FC, fibrillar center; N, nucleus; nm, nuclear membrane; Nu, nucleolus. Scale bars are indicated.

Saito et al., 1969, Ciampor, 1972; Compans and Dimmock, 1969; Shaw and Compans, 1978; Yoshida et al., 1981). No other noteworthy cytoplasmic modifications were detected, except for the budding MO viruses at the cellular membrane (data not shown).

Chicken embryo fibroblast (CEF) cells infected with MO virus were also investigated (**Supplementary Fig. 2**). During infection, when nucleoprotein localization is mainly cytoplasmic (**Supplementary Fig. 2C**), a major nucleolar remodeling was also observed in CEF. Similarly to infected A549 cells, these modifications were associated with a strong accumulation of dense round-shaped bodies (**Supplementary Fig. 2A**, indicated by stars, panels a4–a6) replacing the FC and DFC. Moreover, striated structures were also observed within the nucleus and displayed similar features to those detected in infected A549 cells (**Supplementary Fig. 2B**). Depending of sections, irregular dense inclusions surrounded with globular structures around their borders, were also detected within the cytoplasm (data not shown).

These data indicate that similar modifications of the host architecture and structures are induced in both human and avian cells infected by the MO virus. Furthermore, quite similar modifications of A549 and CEF ultrastructure were also observed with two other viruses from the same H3N2 lineage, A/Panama/2007/99 and A/Brisbane/10/2007 (data not shown). Altogether these results suggest a likely significant specificity for these H3N2 induced cellular alterations, which could be considered as a cellular signature of some contemporary H3N2 strains.

Each influenza A virus tested induced a specific remodeling of the host cellular ultrastructure

We further investigated whether different other influenza A subtypes lead to similar or diverse alterations of the host architecture. For this purpose, A549 cells were infected with human A/Lyon/969/09H1N1 (pdm2009), A/New Caledonia/20/99

(H1N1), A/Singapore/4/57 (H2N2) and avian A/Finch/England/2051/94 (H5N2), A/Turkey/582/2006 (H5N1) and A/Chicken/Italy/2076/99 (H7N1) influenza viral strains.

Despite their specific host-range restriction (Naffakh et al., 2008), all viruses tested in this study efficiently infected A549 cell culture at 37°C, as we previously reported (Josset el al., 2010). In this context, there was evidence of comparable kinetics of productive viral replications for all the viruses (**Supplementary Fig. 3A**). Moreover, at 24 hpi, a time corresponding to spreading infection for all these viruses, immunofluorescence labeling revealed similar patterns of NP localization within infected cells (**Supplementary Fig. 3B**).

The pandemic H1N1 virus (pdm2009) also induced a complete remodeling of the nucleolus with a different pattern to that observed in MO-infected cells. In a large majority of infected cells, the nucleoli appeared as a condensed compartment harboring heterogeneous granular components while lacking the other regular sub-domains FC and DFC (Fig. 3A, panels a–a1). In addition, numerous tubular structures were observed located either inside or in the vicinity of the nucleolar compartment (Fig. 3A, panels a1–a2, arrowheads). These virally induced entities were widely dispatched throughout the nucleoplasm (Fig. 3A, panels a–a2 and data not shown), as recently observed in lung tissue from patients who died of pandemic H1N1 (Goldsmith et al., 2011). The general organization of these tubular structures was similar in shape to that induced by the MO virus (Fig. 2), despite being larger in terms of both diameter (60–90 nm) and length (maximal length approaching 1 mm) (Fig. 3A, panel a3). In addition, dense inclusions of irregular shape and associated to seemingly ribosomes were also observed within the cytoplasm of H1N1 infected cells (data not shown).

Intriguingly, marked differences in viral remodeling of the cell architecture were observed during infection with two other human viruses (A/Singapore/4/57H2N2 and A/New Caledonia/20/99H1N1), corresponding to different features of nucleoli disruption and other diverse types of virally induced structures (**Supplementary Fig. 4**). It should be noted that MO-associated nucleolar round-shaped bodies and tubular striated structures were never observed with these viruses, even at very late stages of infection (data not shown).

Strong disparities were also noted with avian viruses. The A/Finch/England/2051/94 (H5N2) (FI) virus progressively led to a particular and very specific signature of infected A549 cells (Fig. 3B and **Supplementary Fig. 5**). The nucleolar alterations

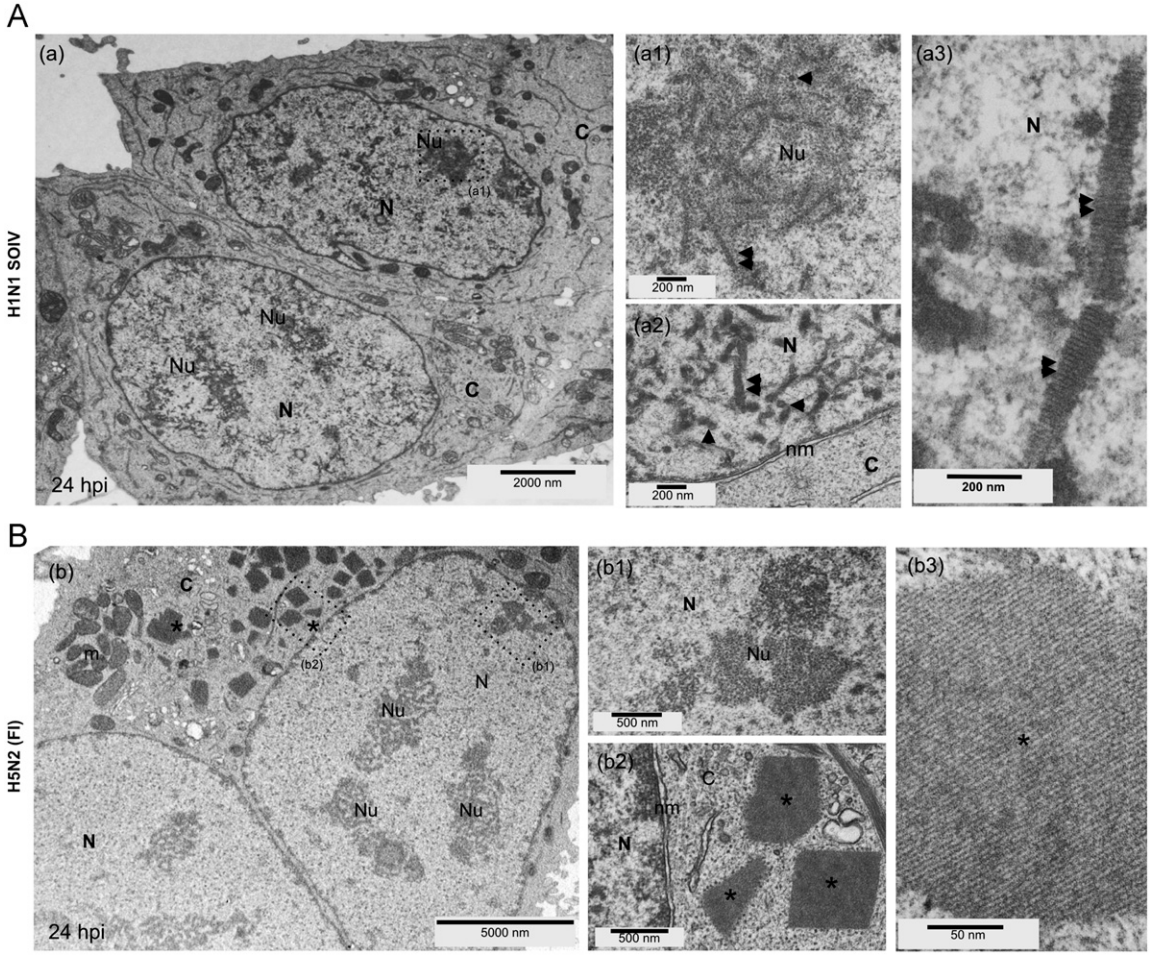

Fig. 3. Human H1N1 pdm2009 and avian FI viruses each alter the host cell ultrastructure with their own specific signature. Glutaraldehyde fixation and Epon embedding. A549 cells were infected with human pandemic A/Lyon/969/09H1N1 (MOI 0.5) (A panels a–a3) and avian FI (MOI 1) (B panels b–b3) viruses, as indicated. General remodeling of nucleolar and nuclear architectures and cytoplasmic modifications were observed at 24 hpi. All different virally induced structures are pointed out with an asterisk or double arrowheads. Transversal (arrowhead) and longitudinal (double arrowhead) views of H1N1 associated tubular structures are shown at higher magnification (enlargement of frames) in panel (a3). The FI-induced cytoplasmic polygon shaped structures harboring a crystalline-like aspect (asterisk) are presented in longitudinal section in panels (b2–b3) and with high magnification (C). C, cytoplasm; m, mitochondria; N, nucleus; nm, nuclear membrane; Nu, nucleolus. Scale bars are indicated.

observed included a complete segregation of regular components with no formation of any additional obvious structures within the nucleus (Fig. 3, panel b1). However, numerous polygonal-shaped inclusions were accumulating within the cytoplasm of a very large majority of infected cells (Fig. 3B, asterisks). Observed from earlier stages of infection (6 hpi), these structures increased in size and number as the infection progressed to the late steps (**Supplementary Fig. 5**). At higher magnifications and depending on the section, these particular entities displayed a regular arrangement of striations with two different shades and resembled crystalline-like inclusions (Fig. 3B, panels b2 and b3). In longitudinal sections, the interstriae distance was found to be 8.4 ± 0.5 nm (mean $\pm$ SD; $n=25$) (Fig. 3, panel b3). In cross section, these structures appeared to be formed by the regular close arrangement of tubules of 9.8 ± 0.7 nm in diameter (mean $\pm$ standard deviation, SD; n, number of independent measurements in different cross-sectional areas $=20$).

It must be mentioned that quite a similar dynamic signature was also observed in FI-infected CEF cells, particularly concerning the presence of these crystalline-like structures, (data not shown). To our knowledge, these polygonal-shaped inclusions have never before been described and could be considered as a specific feature of the FI virus. This hypothesis is supported by the observation of A549 cells infected with some other avian viruses like A/turkey/582/2006 (H5N1) and A/chicken/Belgium/2003 (H7N7), which present distinct cellular ultrastructural modifications (**Supplementary Fig. 4**, panels c and d). Importantly, the FI associated polygonal-shaped inclusions have not been observed with these latter viruses.

Overall, our results are summarized in Table 1 and reveal a strong heterogeneity in viral alterations of the host architecture and the formation of a large number of specific and diversified structures, as though each virus should be associated with a specific cellular signature of infection.

In order to identify the viral components involved in host cell remodeling and investigate the significance of some specific structures, we further focused our analysis on the genetically diverse MO and FI viruses and their very distinguishable signatures.

NS and M contribute to the formation of structures unique to the MO and FI cellular signatures

Transient expression of NS and M gene segments are required but not sufficient for the formation of viral structures

As a first explorative approach, we transfected A549 cells with reverse genetics pHW2000 plasmids carrying the complete set of MO gene segments in order to examine by EM any alterations of the cellular architecture related to those previously observed during MO infection. We used pHW2000 plasmids since they allow the expression of both viral proteins and the corresponding viral RNA (vRNA) thus permitting us to conduct our investigations in a context resembling infection and in which viral ribonucleoprotein complexes could be assembled, as previously demonstrated by Yamanaka K et al. (Yamanaka et al., 1990; Huang et al., 2001). For all experiments, we verified the expression of proteins by western blot experiment at 48 hours post-transfection (data not shown).

Transfection of empty pHW2000 plasmids had no effect on cellular ultrastructure (data not shown). Similarly, expression of the NP gene segment had no significant effect on nuclear or nucleolar ultrastructures, as shown in Fig. 4 (panels a–a2). Only a change in the general aspect of the nucleoplasm, which became heterogeneous with dispatched dense materials, was noticed; this was likely the result of nuclear accumulation of plasmid and/or NP protein.

In contrast, the co-expression of NP and RdRp coding gene segments induced a complete fragmentation of the nucleolus without the formation of other particular structures related to infection, as shown in Fig. 4 (panels b–b2). On the other hand, the additional co-expression of the NS gene segment resulted in the formation of numerous electron dense round-shaped bodies within the remnant nucleolar compartment of 60% of transfected cells (Fig. 4, panels c–c2, indicated by stars). This pattern was very similar to the nucleolar signature depicted previously for MO infection (compare with Fig. 2). Furthermore, in 40% of transfected cells, the supplementary over-expression of the M gene segment was associated with the formation of nuclear striated tubular structures (Fig. 4, panels d–d2, arrowheads), harboring similar characteristics to those induced by the MO virus (compare with Fig. 2).

Table 1
Summary of viral cellular signatures characterized by electron microscopy. For each viral strain, specific cellular remodeling and virally induced structures are reported. References to figures or bibliography are indicated (n.d., non determinated).

Viral strains	Cellular signatures			References
	Nucleolus	Nucleus	Cytoplasm	
A/Moscow/10/99H3N2 (MO)	Disappearance of FC and DFC Dense round-shaped bodies	Striated tubular structures	Ribosomes rounded dense inclusions	Fig. 2 **Supplementary Fig. 1, Fig. 2**
A(H1N1)pdm2009	Disappearance of FC and DFC Striated tubular structures	Numerous and large striated tubular structures	Ribosomes rounded dense inclusions	Fig. 3**A**
A/WSN/33H1N1	Segregation of nucleolar sub-domains	Striated tubular structures	Ribosomes rounded dense inclusions	Kopp et al. (1968) Ciampor (1972) Compans and Dimmock (1969)
A/New Caledonia/20/99H1N1	large amorphous-like compartment surrounded by extended network of dense material	Overall dispatched dense round-shaped bodies	n.d	**Supplementary Fig. 4**
A/Singapore/4/57H2N2	Segregation into dispersive granular materials and dense body	Dense globular structures	n.d	**Supplementary Fig. 4**
A/Finch/England/2051/94H5N2 (FI)	Segregation of nucleolar sub-domains	n.d	Polygonal-shaped crystalline-like inclusions	Fig. 3**B**
A/turkey/582/2006H5N1	Amorphous compartment with fibrilar dense material at periphery	Large heterogeneous and irregular-shaped structures	n.d	**Supplementary Fig. 4**
A/chicken/Belgium/2003H7N7	Unique dense condensed compartment	Striated tubular structures	n.d	**Supplementary Fig. 4**

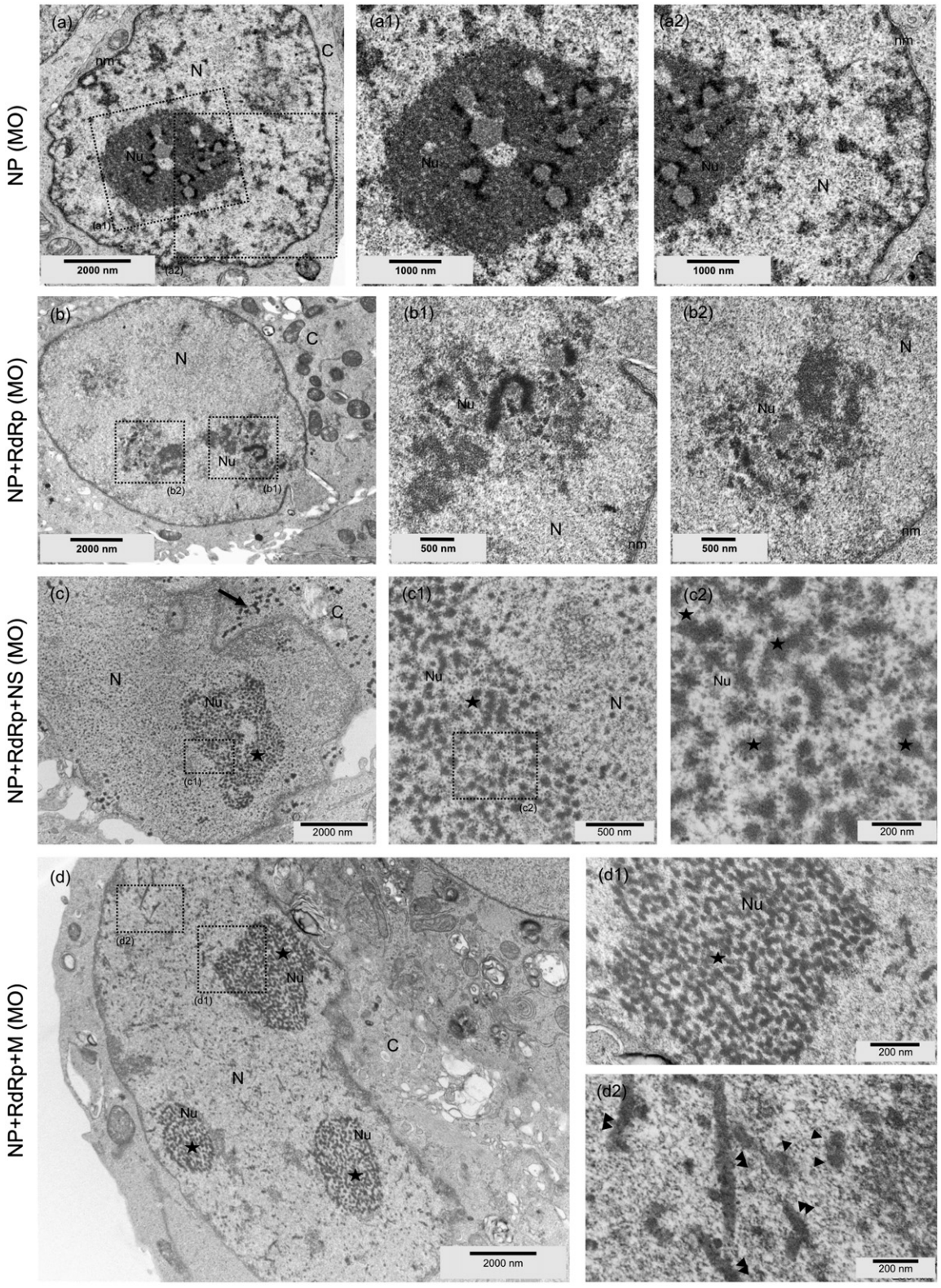

Fig. 4. MO virally induced structures require NS and M expression. Glutaraldehyde fixation and Epon embedding. A549 cells were co-transfected with pHW2000 plasmids containing NP, RdRp, NS and/or M genomic segments of MO virus, as indicated, and their general aspects were observed for 48 hours post-transfection. In contrast to NP transfected cells (panels a), a complete disruption of the nucleolus is observed when NP and RdRP are co-expressed (b–b2). Additional expressions of NS (panels c–c2) and M (panels d–d2) induce the formation of electron-dense round-shaped bodies (stars) within the nucleolar compartment, cytoplasmic dense inclusions (arrow) and nucleoplasmic rod-like structures (arrowheads), as respectively observed in enlarged frames. C, cytoplasm; N, nucleus; nm, nuclear membrane; Nu, nucleolus. Scale bars are indicated.

Interestingly, both expression of NS or M gene segments alone did not induce the formation of the related structures (data not shown), suggesting the possible requirement of a stronger expression than the one obtained with pHW2000 plasmid in order to induce cellular remodeling in a similar way to that observed in the context of viral infection. Similar results were noticed with ectopic expression of FI segments (data not shown).

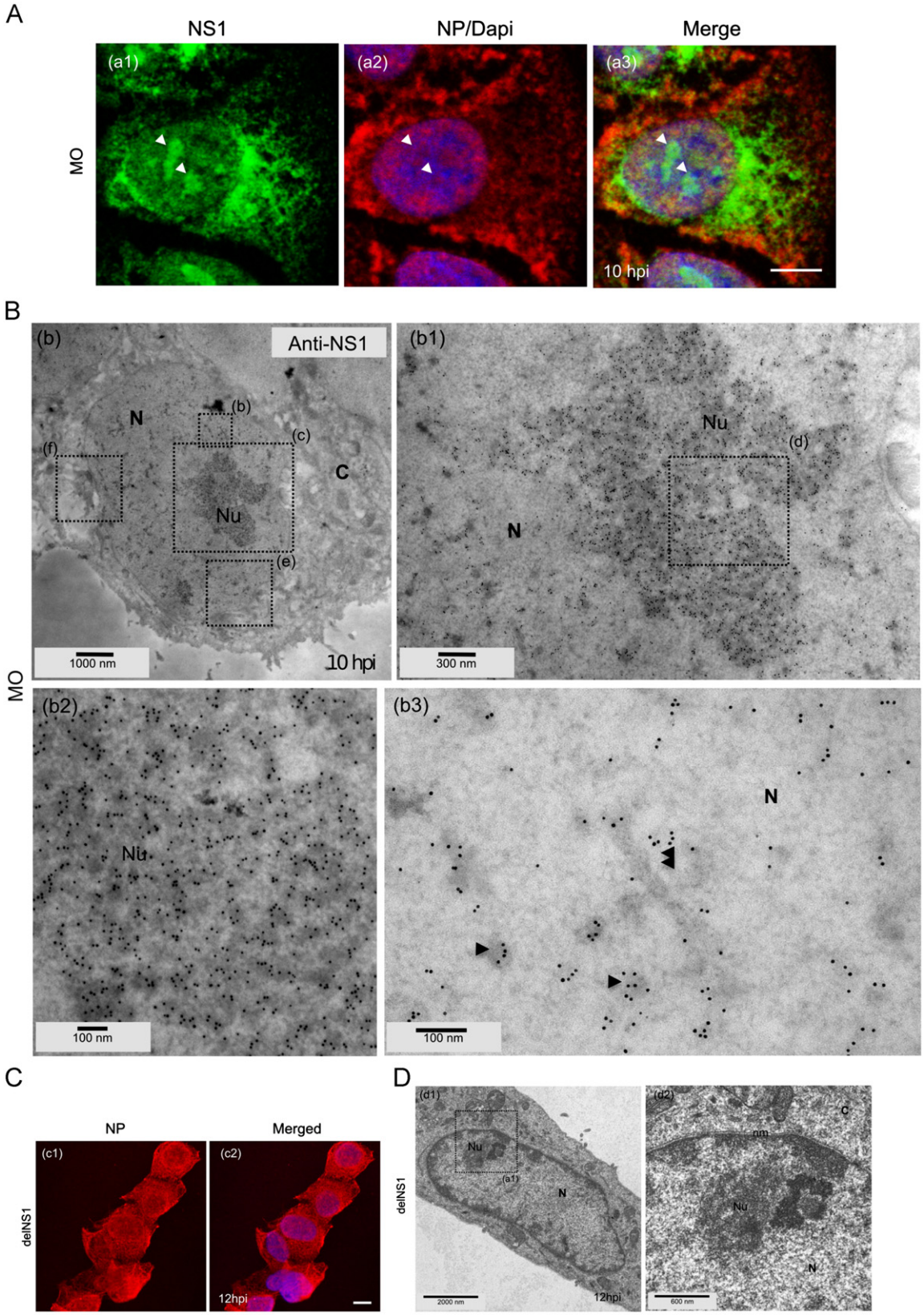

Fig. 5. The formation of nucleolar electron-dense round-shaped bodies depends on MO NS1 expression. A. Immunostaining of MO infected A549 cells (MOI 1). At 10 hpi, immunolabeling was performed with anti-NS1 (green) and anti-NP (red). Nuclei were stained with DAPI (blue). Nucleolar compartments are indicated by arrowheads. Panel (a3) is the merged confocal images from each fluorochrome. Scale bars, 10 μm. B. Formaldehyde fixation and Lowicryl embedding. At 10 hpi, MO-infected A549 cells were fixed and processed for anti-NS1 immunogold labeling. Gold particles (10 nm) intensely and homogenously surround the electron dense round-shaped bodies (stars) within the remodeled nucleolar compartment (b1–b2). Some striated structures are poorly labeled within nucleus (arrowheads) as observed in panel (b3). C, cytoplasm; N, nucleus; Nu, nucleolus. Scale bars are indicated. **C.** A549 cells were infected with delNS1 virus for 12 hpi. NP immunostaining was performed (red) and nuclei were stained with DAPI (blue). Panel (c2) is the merged confocal image from each fluorochrome. Scale bars, 10 μm. **D.** Glutaraldehyde fixation and Epon embedding. At the same time point post infection, a strong disruption of the nucleolar compartment is observed (d1–d2). Moreover, no striated tubular structure is detected within the nucleoplasm. C, cytoplasm; N, nucleus; nm, nuclear membrane; Nu, nucleolus. Scale bars are indicated. (For interpretation of the references to color in this figure legend, the reader is referred to the web version of this article.)

Anyway, all these results lead us to focus our investigations on the proteins encoded by the NS and M gene segments in a viral context. For this purpose, we first controlled that viral proteins were comparably expressed during the time course of the MO and FI infections (**Supplementary Fig. 6**).

NS1 has a direct role in the host nucleolar remodeling observed during MO infection

We investigated the sub-cellular localization of MO NS1 in a viral context by immunostaining (Fig. 5). As expected for an NS1 protein containing a Nucleolar Localization Signal (NoLs) (Melen et al., 2007), we confirmed the nucleolar localization of MO NS1 in 87% of infected cells in addition to its cytoplasmic accumulation at 10 hpi (Fig. 5A). In accordance with these observations, EM investigations have indicated a strong anti-NS1 immunogold labeling of the nucleolar dense round-shaped bodies specific to the MO infection (Fig. 5B). In contrast, only lower or no NS1 staining of nucleoplasm and viral striated tubular structures were observed respectively, thereby confirming the specificity of the MO NS1 labeling for the modified nucleolar architecture (Fig. 5B). No anti-NEP labeling was associated with the dense

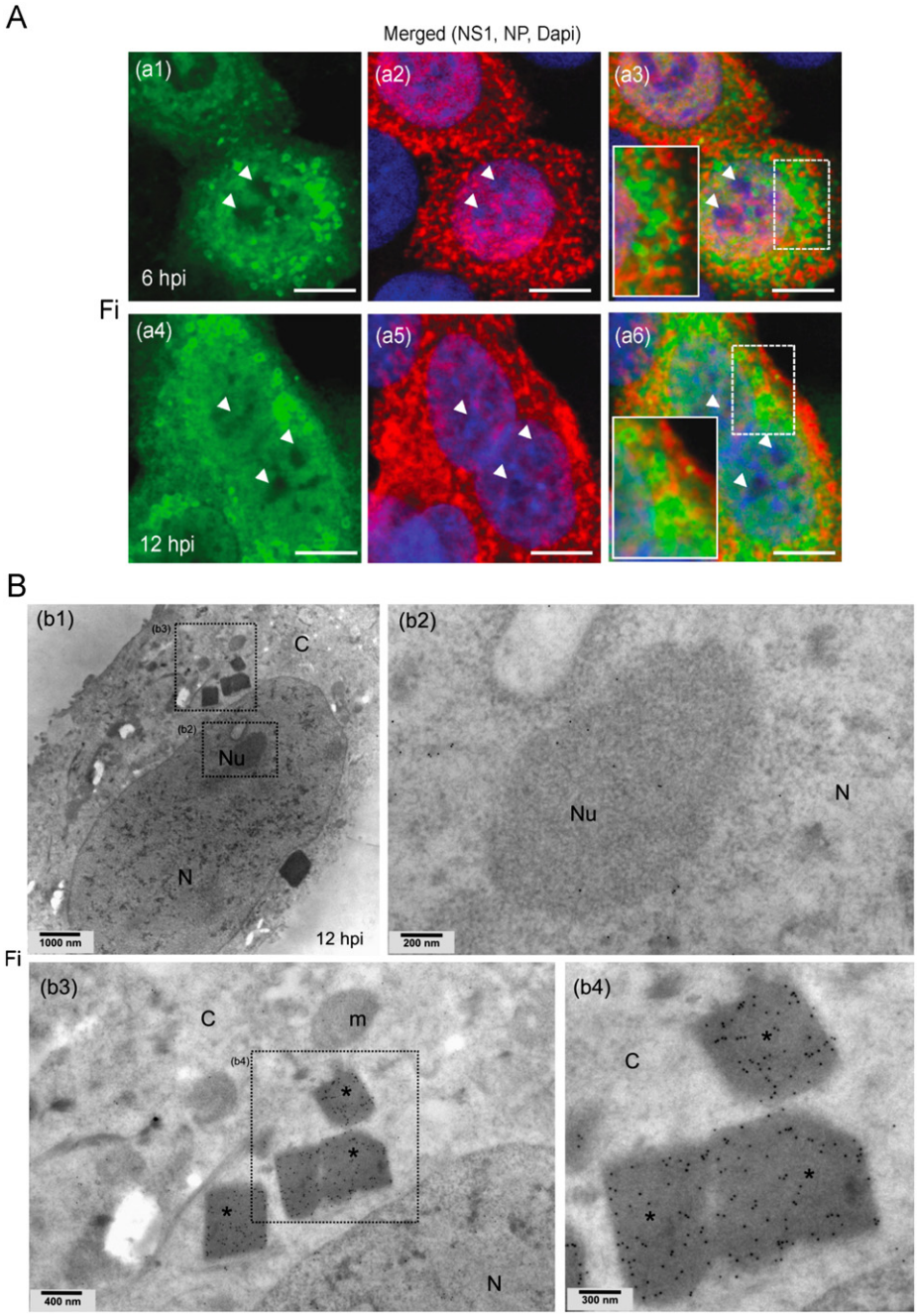

Fig. 6. FI NS1 is strongly associated with cytoplasmic crystalline-like structures during infection. A. Immunostaining of FI-infected A549 cells at 6 and 12 hpi (MOI 2) with anti-NS1 (green) and anti-NP (red) antibodies. Nuclei were stained with DAPI (blue). Panels (a3) and (a6) are the merged confocal images from each corresponding fluorochrome. Enlargement of the frame depicts the NS1 stained crystalline-like structures. Nucleoli are indicated by arrowheads. Scale bars, 10 μm. B. Formaldehyde fixation and Lowicryl embedding. At 12 hpi, FI-infected A549 cells were fixed and processed for immunogold labeling with anti-NS1 and the appropriate secondary antibodies. Whereas a weak staining is observed within the nucleolus (a2), gold particles intensely and homogenously surround the crystalline-like polygon shaped structures within the cytoplasm (a3–a4, asterisk). C, cytoplasm; N, nucleus; Nu, nucleolus. Scale bars are indicated. (For interpretation of the references to color in this figure legend, the reader is referred to the web version of this article.)

round-shaped bodies within the nucleolus of infected cells (data not shown).

Further investigations were carried out by generating a functional recombinant H3N2 delNS1 virus in which the NS1 gene was completely deleted by reverse genetics, as previously realized in a PR8 background (Garcia-Sastre et al., 1998). We characterized the recombinant delNS1 virus by validating the lack of NS1 expression and determining the level of cell infection by immunofluorescence staining (**Supplementary Fig. 7**).

To validate our experimental approach, we confirmed that the MO virus generated by reverse genetics induced a cellular signature (data not shown) similar to that reported above with the corresponding prototype strain (Fig. 2). At late stages of infection, indicated by the principally cytoplasmic localization of NP (Fig. 5C), the delNS1 virus led to a nucleolar signature that clearly differed from that observed both with parental and MO viruses at similar late stages of infection. Indeed, the delNS1 virus was shown to induce only the segregation of the sub-nucleolar compartment without any associated formation of the characteristic dense round-shaped bodies (Fig. 5D, panel d2). Interestingly, neither striated tubular structures nor cytoplasmic dense inclusions could be detected within delNS1-infected cells (Fig. 5D).

Altogether, these results clearly demonstrate the direct involvement of NS1 protein in the formation of several features of the MO virus cellular signature and particularly in the ultrastructural remodeling of the host nucleolus.

FI NS1 Is not accumulated within nucleoli but rather associated with the FI-associated cytoplasmic crystalline-like structures

Concomitantly, we studied the sub-cellular localization of FI NS1 in A549 infected with the FI prototype strain (Fig. 6A). Both at 6 and 12 hpi, immunofluorescence staining showed an absence of nucleolar accumulation of FI NS1 in 100% infected cells we observed. In contrast, the outline of the FI specific polygonal-shaped structures within the cytoplasm was intensely labeled. Immuno-EM observations after staining with anti-NS1 antibody were in accordance with above results in that they showed very low amounts of gold particles within nucleoli of FI-infected cells (Fig. 6B, panel b2) and an intense and systematic staining associated with the crystalline-like inclusions characteristic of FI infection (Fig. 6B, panels b3–b4). Partial discrepancy between immunofluorescence and EM staining could be explained by the inaccessibility of antibodies inside inclusions, whereas NS1 should be exposed at their surface on the EM slice. Such a notion would support a compact and solid structure for inclusions in line with their obvious crystalline-like aspect.

Altogether, these data indicate that FI NS1 protein is mainly associated with the crystalline-like inclusions in the context of infection and underline the relevance and specificity of the above finding concerning MO NS1 sub-cellular pattern of localization. Moreover, the absence of FI crystalline-like structures in cells infected by all other viruses tested favors an influential role played by the FI NS1 protein on the FI virus-specific cellular signature.

MO-specific striated structures are associated with M1 protein

Based on the results of prior transient expression experiments (Fig. 4, panels c), we also examined the sub-cellular localization of M1 proteins in both MO and FI-infected cells by immuno-EM, at late stages of infection. At 12 hpi, immunogold particles were strongly associated with the numerous striated tubular structures found scattered throughout the nucleoplasm of MO-infected cells (Fig. 7, panel a). This labeling was distributed evenly around the

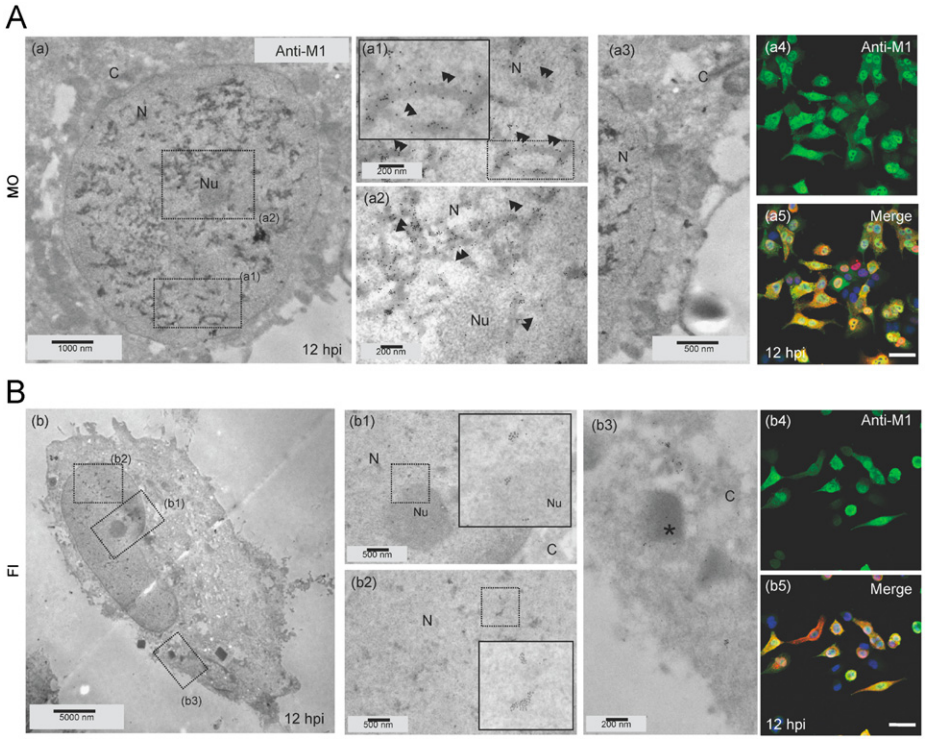

Fig. 7. M1 is mainly associated with the MO-induced striated rod-like structures. Formaldehyde fixation and Lowicryl embedding. (a) A549 cells were infected with MO (MOI 1) and processed at 10 hpi for immunogold labeling with anti-M1 antibody. Gold particles accumulated around the striated tubular structures (double arrowhead) within the nucleus as observed in panels (a1–a3). At the same time point following infection, immunofluorescence staining shows a mainly peripheral nuclear pattern for M1 (green) with some punctuated cytoplasmic accumulation (a4). Subcellular localization of NP is shown in the panel (a5). Nuclei were stained with DAPI (blue). Panels (a4) and (a5) are the merged confocal images from each fluorochrome. Bars, 15 μm. (For interpretation of the references to color in this figure legend, the reader is referred to the web version of this article.)

structure and probably reflected exposed antigenic sites (Fig. 7, enlargement in panel a1, double arrowheads). Nucleoli of MO-infected cells were devoid of M1 labeling although a diffuse signal was observed within the cytoplasm that was confirmed by confocal microscopy (Fig. 7, panels a3 and a5, respectively).

At similar stage of infection for the FI virus, as indicated by NP and M1 immunofluorescent staining (Fig. 7), M1 protein was neither associated with the host nucleolus nor with viral structures such as the cytoplasmic crystalline-like inclusions found within the cytoplasm (Fig. 7, panels b1–b3). In contrast, several clusters of gold particles were scattered within the nucleoplasm of infected cells and showed no link with any defined sub-cellular entity (Fig. 7, panels b1–b3).

Together with the absence of M1 labeling in mock-infected A549 control cells (data not shown), our data suggest that the MO-induced striated tubular structures are specifically related to the M1 protein originating from the MO virus. These results are in a reasonable agreement with results obtained by Ruigrok and colleagues, who reported the polymerization of solubilized M1 protein as an ordered coil ribbon structure (Ruigrok et al., 2000) and investigations by Gomez-Puertas et al., describing very similar filamentous structures in a context of transient expression of M1 from other H3N2 virus (Gomez-Puertas et al., 2000).

Signatures of FI/MO reassortant viruses depend on the viral origin of NS and M genomic segments

Above results with M1 were in line with those concerning NS1 and suggest that viral origin of proteins may determine the specific features of each virus cellular signature. To support this contingency, we used MO and FI reverse genetics systems to produce a series of reassortant viruses containing various NS and M genomic constellations, as described in Fig. 8A.

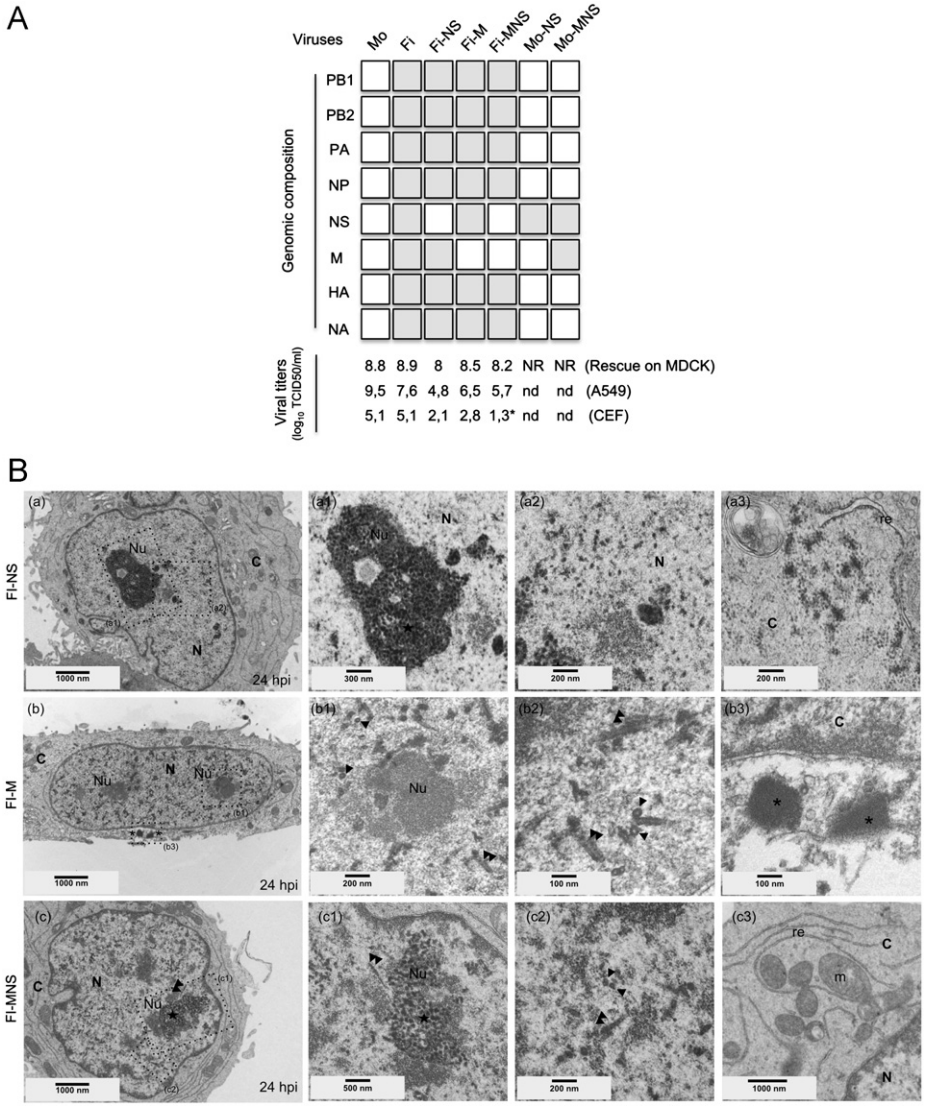

Fig. 8. A. **Genomic composition and replication kinetics of recombinant viruses generated by reverse genetic.** Parental MO and FI sources of each segment are indicated for each reassortant virus generated by reverse genetics. MO-NS, MO-MNS viruses were not rescued (NR) on MDCK cells in 3 independent experiments. Production stock titers of MO, FI, FI-NS, FI-M and FI-MNS viruses are indicated. Rescued viruses were cultured on A549 and CEF cells and titers (log_{10} DICT50/ml) are indicated at 55 hpi. ND*: viral titers are under the threshold of sensitivity (1.3 log TCID50/ml). B. **Virally induced structures are dependent on the MO or FI origin of the NS and M segments**. A. Glutaraldehyde fixation and Epon embedding. A549 cells were infected (MOI 1) with reassortant viruses FI-NS (a–a3), FI-M (b–b3) and FI-MNS (c–c3) and general remodeling of the host ultrastructure was observed at 24 hpi. Nucleolar dense round-shaped bodies (stars) are observed in cells infected with viruses containing NS segment from MO (compare a1, c1 with b1). Striated tubular structures are associated with infection of virus containing the M segment from MO (compare b2, c2 with a2). Cytoplasmic polygon shaped structures are observed with the FI-M virus (panel b3) whereas not with other viruses (panels a3 and c3). C, cytoplasm; m, mitochondria; N, nucleus; Nu, nucleolus; re, reticulum. Scale bars are indicated.

Virus recovery from pHW2000 plasmids transfection was evaluated by titration after three passages on MDCK cells and referred to as rescue efficiency (Rescue on MDCK, Fig. 8A), as previously described (Moulès et al., 2011). Not all the constellations resulted in efficient viral replication. The introduction of heterologous NS and/or M segments from FI within the MO backbone was deleterious for replication of the corresponding reassortant MO-NS and MO-MNS viruses. In contrast, inverted reassortments were achieved within the FI backbone and a viral yield titer for FI-NS, FI-M and FI-MNS viruses was measured (Fig. 8A). The incompatibilities at the protein and/or genomic level, as previously reported for other reassortants between human and animal strains (Jackson et al., 2009; Li et al., 2008; Fournier et al., 2012) may explain our results obtained with MO-NS and MO-MNS.

We further compared the growth kinetics of recombinant viruses by inoculating both A549 and CEF cells at a MOI of 10^{-2} and monitored the release of infectious virus progeny into the supernatant up to 55 hpi (Fig. 8A). MO and FI viruses replicated with good yields in A549 cells but with lower titers in CEF cells. The viral titers of reassortant viruses were quit similar to those measured for FI-M, FI-NS and FI-MNS viral titers being respectively about 2 and 4 log lower than those observed for FI virus in A549 cells. Similar results were also obtained in CEF infected cells with a more drastic reduction of viral titers for the reassortant viruses (Fig. 8A). Interestingly, while FI-MNS virus had similar growth property to FI-NS and FI-M viruses in A549 cells, no significant levels of infectious particles were detected from CEF infected cell supernatants neither at 55 hpi (Fig. 8A), nor at later times (data not shown).

Subsequently, we carried out morphological observations on A549 cells infected with reassortant FI-NS, FI-M and FI-MNS viruses (Fig. 8B) in order to determine the associated cellular signatures. For this purpose, we first confirmed that recombinant FI virus was associated with a similar signature to that reported above with the prototype strain (data not shown). The different patterns of viral protein were also monitored at 8 and 24 hpi by immunostaining (**Supplementary Fig. 8**).

FI-NS virus induced the formation of both dense round-shaped bodies within the remnant nucleolus and ribosome-surrounded dense inclusions within the cytoplasm (Fig. 8B, panels a1 and a3, respectively). These features are specific to the cellular signature induced by the NS1 protein of MO (compare with Figs. 2 and 5). In addition, the FI-NS virus did not induce the formation of the cytoplasmic crystalline-like structures specific to the FI NS signature. Similar observations were also made with the FI-MNS virus (Fig. 8B, panels c). The sub-cellular localization of NS1 proteins investigated by immunofluorescence staining (**Supplementary Fig. 8**), were in accordance with EM observations and confirmed NS1 associated patterns for each reassortant virus that depended on the MO origin of the NS segment. Furthermore, for the FI-NS virus, none of the MO-specific striated tubular structures were ever detected within the nucleus of infected cells (Fig. 8B, panels a–a2 and data not shown).

In a similar way, we noticed that the cellular signature of the FI virus had been conserved in the FI-M virus (compare to Fig. 3) in that the reassortant virus induced the complete segregation of nucleolar components and polygonal shaped crystalline-like structures within the cytoplasm (Fig. 8B, panels b1 and b3, respectively). However, one singularity was observed and concerned the formation of nuclear striated tubular structures (Fig. 8B, panels b2), which are associated with the MO M1 protein (compare with Figs. 2 and 7) expressed by this reassortant virus. Finally, the study of FI-MNS infection revealed all features previously described for MO cellular signatures relating to both NS1 and M1 proteins (Fig. 8B, panels c–c2) and was devoid of any FI characteristics, notably the NS1 associated crystalline-like structures (Fig. 8B, panel c3).

Altogether, our results demonstrate that the viral origin genomic segments coding NS1 and M1 proteins, could constitute important determinants in the remodeling of the host cellular architecture during infection, and could have putative effects on replicative efficiency and virus viability with regard to results of virus recovery and titers (Fig. 8).

Discussion

We investigated four representative circulating human influenza viruses and three low or high pathogenic avian influenza viruses for their impact on the host architecture of both human (A549) and chicken (CEF) cells. Our results reveal that each influenza A virus tested was associated with a specific cellular signature mainly comprising marked and distinct modifications of the host nuclear architecture and the formation of characteristic and/or common viral structures, independently of the origin of the host cell.

Moreover, the study of recombinant viruses indicated a clear correlation between the viral cellular signatures and the viral genomic constellations, with a marked role of NS1 and M1 proteins. While we are unable to completely rule out other independent effects such as incompatibilities of recombinant viruses at the protein and/or genomic level, as already reported for several reassortant viruses between human and animal strains (Jackson et al., 2009, Li et al., 2008), observed disparities in terms of viral production both in human and avian cells highlight the possibility of a significant functional impact of the virally induced cellular structures on the outcome of infection.

The well-defined compartmentalized organization of the cell nucleus allows the spatial and dynamic coordination of cellular gene expression, and any modifications or defects resulting from environmental stress or injuries are known to have a direct impact on the spatial and temporal cellular transcriptome and proteome (Zimber et al., 2004; Josset et al., 2008). With this in mind, one obvious hypothesis would be that the nuclear environment could be decisive in regulating the replication cycle of viruses (Chan et al., 2000; Amorim and Digard, 2006; Nagata et al., 2008).

Among the heterogeneous virally induced alterations that we reported, a common feature is the systematic and major remodeling of the nucleolar compartment. We suggest that such privileged targeting could reflect the viral alteration or hijacking of the host nucleolar functions; a property shared by several viruses such as DNA viruses, retroviruses and RNA viruses (Hiscox, 2007; Greco, 2009; Munday et al., 2010). In addition, several investigations have reported the modification of nucleolar proteome composition during influenza virus infection (Emmott, et al., 2010) and the interactions between several nucleolar proteins and influenza vRNP and polymerase complex (Mayer et al., 2007; Murayama et al., 2007). Moreover, high throughput RNAi screening studies have highlighted the functional involvement of many nucleolar and ribosomal factors in viral replication (König et al., 2010, Karlas et al., 2010). Other studies have also investigated the functional relationships between influenza viruses and the nucleolus by demonstrating the requirement of NP NoLS for efficient viral transcription and replication (Ozawa et al., 2007), suggesting the subtype dependent interaction between NS1 and nucleolin as a modulating factor determining virulence (Murayama et al., 2007).

Our results are in accordance with these investigations and lead us to propose that the specific nucleolar dense round-shaped bodies associated with the NS1 protein from the H3N2 virus may

constitute a morphological phenotype of such strain-specific properties. The high diversity of the nucleolar modifications that we observed in cells infected with different viruses or in the context of the H3N2 delNS1 virus, is in accordance with such a hypothesis. In this context, the presence/absence of NoLs in NS1 protein from different viral origins needs to be investigated in relation with property to remodel the nucleolar compartment. Further studies are required to decipher the molecular significance of the "NS1 nucleolar experience" to both viral replication and host nucleolar metabolism. Immuno-staining and *in situ* hybridization experiments should be carried out in order to locate other putative viral components in the formation of these virally induced structures. An exciting challenge will be to functionally connect nucleolar remodeling of infected cells and viral transcription and/or replication processes. The nucleolar fragmentation induced by transfection-based intracellular reconstitution of MO or FI replication/transcription complexes (Fig. 4, panels a and data not shown) and nucleolar localization of NP (Ozawa et al., 2007), PB1 and PB2 (Emmott et al., 2010 and our unpublished data) as well as vRNA and cRNA of infectious salmon anemia virus (ISAV), which belongs to the family *Orthomyxoviridae* (Goic et al., 2008), further support such a concept.

Alternatively, as nucleolar architecture and functions are closely interconnected, it will be interesting to evaluate the role of nucleoli in ribosome biogenesis and other extra-ribosomal activities (e.g. mediation of cell-stress responses, regulation of cell growth) (Andersen et al., 2005; Visintin and Amon, 2000) in the context of virally induced alterations of nucleolar ultrastructure. These investigations would explain the reason behind the observed heterogeneity in the remodeling of nucleoli among the different viruses tested in the present study. Sub-nuclear localization of related functional nucleolar factors must be investigated in regard to viral remodeling. Moreover, the measure of endogenous RNA poll activity and the evaluation of the outcome of maturation/assembling of pre-ribosomal particles will give useful information on a conceivable upstream molecular mechanism engaged by influenza viruses for the alteration of ribosome biogenesis which could contribute to the viral hijacking of the host translational machinery (Kash et al., 2006).

Another structural phenotype of infection, which could also illustrate well the viral misappropriation of cellular translation, would be the cytoplasmic aggregates of dense material observed within MO-infected cells and usually surrounded by ribosomes at their borders. Similar observations were also reported in WSN-infected cells and characterized as accumulations of NS1 in association with RNA (Morrongiello and Dales, 1977; Yoshida et al., 1981). Interestingly, the FI associated crystalline-like inclusions, while visibly different, also harbor an intense NS1 labeling and are also closely surrounded by numerous ribosomes, as observed in favorable sections of infected cells (data not shown). In order to link such virally induced structures to the translational machinery, further immunostaining and immunolabeling will be necessary focusing on the study of host initiation factors and viral mRNA, for example. Different NS1-associated cellular structures could potentially have diverse functional impacts on the host translational machinery, a hypothesis which needs further investigations.

NS1 is widely considered as the common factor by which all influenza A viruses antagonize multiple signaling pathways and antiviral mechanisms of the innate immune system (Krug et al., 2003; Hale et al., 2008; Wolff and Ludwig, 2009).

A recent study demonstrated a strain-specific contribution of NS1-activated PI3K signaling, which may depend on intracellular localization of NS1 to possible "signaling platform sites" (Ayllon et al., 2012). These sites could correspond to specific viral structures that remain to be identified. It could be interesting to investigate NS1 associated paracrystalline structures we characterized in this context.

The localization of antiviral components, such as PKR, RNAse L and TRIM25/RIG-I factors should be also investigated with respect to NS1-associated cytoplasmic cellular structures. In addition, the study of some NS1 mutated or truncated viruses of interest, for example those partially deleted for the RNA binding domain (Hoffmann et al., 2000) or for species-specific virulence domains like the NoLS/NES (Volmer et al., 2010) or PDZ-binding motif (Soubies et al., 2010; Zielecki et al., 2010; Keiner et al., 2010), would be very informative.

To our knowledge, virally induced cellular modifications, similar to the FI-induced crystalline-like inclusions observed in both human and avian cells presented here, have never been described previously. Interestingly, NS1 from this strain belongs to the B allele family, which was not described in mammalian-adapted isolates, unlike avian A allele subtypes (Zohari et al., 2010). Based on our observations of similar structures within cells infected with another allele B virus, H7N1 A/Chicken/Italy/2076/99 (data not shown), we can hypothesize that crystalline-like structures could constitute the phenotypic signature of NS1 allele B viruses. It will be necessary to further investigate several other allele B viruses to support this hypothesis. Considering that A and B alleles harbor different abilities to counteract innate immunity (Zohari et al., 2010), thereby affecting their adaptation and virulence properties, it will be also legitimate to study the interplay of these virally induced crystalline-like structures with host factors, notably those involved in the metabolic pathways controlling inflammatory cytokine signaling. Purification of crystalline-like structure coupled to mass spectrometry analysis would be very useful.

Similar questions concerning the biological significance of M1-associated structures have also been raised by our results. However, the parameters are different from the NS1 entities since the striated tubular structures are shared by genetically diverse viruses including MO, pandemic H1N1, H7N7 and WSN (Ciampor, 1972; Anisimova et al., 1980). The M1 proteins of these latter viruses are relatively conserved with the M1 of the viruses tested and do not harbor any specific amino acid motifs with respect to the M1 protein from viruses unable to induce formation of striated tubular structures, as suggested by protein sequence alignments (data not shown). Moreover, our observations have revealed some heterogeneity in the number, the length and the sub-nuclear localization of the M1-associated structures amongst the different viruses. Moreover, previous study demonstrated the property of H3N2 M1 to intrinsically form such nuclear structures only upon conditions of very high level of protein expression (Gomez-Puertas et al., 2000). Alternatively, additional viral factors could be involved in the formation of M1-associated striated tubular structures that require further characterization by immuno-staining and *in situ* hybridization experiments.

The apparent complex structuring of these M1-associated structures and their very high number within cells in the case for example of pandemic H1N1 infection, suggest their likely functional importance within the host nucleus. In accordance with the M1 localization at the nuclear periphery (Fig. 7), additional EM observations of favorable sections indicated marked accumulation of these striated tubular structures at the top of the nucleus and near the nuclear membrane (data not shown). This could point investigations towards a putative involvement of these M1-related structures in vRNP nucleocytoplasmic trafficking. Indeed, the amino-terminal domain (residues 1–164) of M1 possesses RNA binding domains and an NLS motif, which could be active in self-polymerization and nuclear export of newly made vRNP (Hui et al., 2003). It will be interesting to investigate other viral or cellular factors involved in vRNP export, like NEP protein

(for a review: Boulo et al., 2007) and Hsp70 (Watanabe et al., 2006), in regard to these tubular striated structures. Moreover, the study of some temperature-sensitive (ts) M1 mutants of interest (Liu and Ye, 2004), in particular with mutations in the NLS motif that facilitates M1 binding to vRNP, should allow the detection of M1 associated structures at restricted and permissive temperatures. To our knowledge, only one similar study used ts mutant viruses to analyze variable cellular patterns of infection. Indeed Anisinova and collaborators investigated different thermosensitive (ts) avian viruses defective for transcription and/or replication and reported that some were unable to induce the formation of viral structures at non-permissive temperature (Anisimova et al., 1980), thereby suggesting a possible link between the viral remodeling of the host nucleus and viral replication, as we also postulate here in this study.

In addition to the discovery of several viruses, Electron Microscopy investigations have also made a major contribution to the identification of host–pathogen interactions, especially by allowing the molecular and functional characterization of various viral structures induced by nuclear viruses including adenovirus, herpes simplex and cytomegalovirus (Hiscox, 2006). Our results support the concept that nuclear compartmentalization and its virally induced remodeling could contribute to the regulation of the influenza replication cycle. We now aim to use several approaches to investigate the full range of influenza induced cellular structures to understand the relevance of the heterogeneity shown among viruses and any virus specific characteristic features and as such correlate viral structures with viral function. In this way, based on the strain associated cellular signature, which itself depends on the viral genomic constellation, an exciting hypothesis could be that the viral structures would partially reflect the 'functional equipment' of each virus and allow its characterization in terms of host virulence and adaptability.

Materials and methods

Viruses and cells

Influenza A viral strains A/New Caledonia/20/99 (H1N1), A/Moscow/10/99 (H3N2), A/Singapore/4/57 (H2N2), A/Finch/England/2051/94 (H5N2) and A/Lyon/969/09 (A(H1N1)pdm2009) were obtained from the French national influenza monitoring network GROG (Groupes Régionaux d'Observation de la Grippe, Lyon, France) and the WHO collaborative center NIMR/MRC (kindly provided by Dr. Alan Hay). They were subsequently amplified on MDCK cells (two passages). Virus strains A/chicken/Netherland/2003 A(H7N7) and A/Turkey/582/2006 A(H5N1) were kindly provided by Dr van den Berg (University of Louvain, Belgium) and obtained from the National Reference Center of Turkey, respectively. They were amplified in the same conditions. Virus were cultivated and titered in MDCK cells and stored at −70° C. Viruses H2N2, H7N7 and H5N1 were grown in BSL3 (VirPath laboratory) and BSL4 (Marcel Merieux's laboratory, Lyon) facilities, respectively.

MDCK cells were purchased from Lonza (ATCC, CCL34) and were passaged twice weekly in serum free Ultra-MDCK medium (Lonza) supplemented with 2 mM L-glutamine (Sigma Aldrich), penicillin (225 units/ml) and streptomycin (225 μg/ml) (Lonza). Human pulmonary epithelial (A549) and chicken embryo fibroblast (CEF) cells were propagated in Dulbecco's Modified Eagle's Medium (DMEM, Lonza, Biowhittaker) supplemented with 200 units/ml penicillin, 200 μg/ml streptomycin, 2 mM L-glutamine and 10% fetal calf serum in 25 cm^2 flasks (Falcon, Beckton Dickinson). All cells were maintained at 37 °C with 5% CO_2.

For infection, viruses were inoculated at a multiplicity of infection (MOI) of 1–2 in DMEM supplemented with 200 units/ml penicillin, 200 μg/ml streptomycin, 2 mM L-glutamine and 0.5 μg/ml TPCK-trypsin (Roche diagnostics). After 2 h at 37 °C, the inoculum was removed and replaced by fresh medium. Infected cells were then incubated for different periods of time (6–24 hpi).

For viral kinetics on A549 cells, confluent cells were infected with viruses at an MOI of 0.1 for one hour under a minimal volume of medium at 37 °C. Cells were then overlaid with fresh medium and incubated at 37 °C. Samples of supernatants were harvested at several time points post-infection (p.i.) and stored at −80 °C until end point titration assays (TCID50) in MDCK cells using the Reed and Muench statistical method.

For end point titration, MDCK cells were infected at a MOI of 0.0001 TCID50/cell. After a 1-h viral adsorption period, cells were overlaid with Eagle's minimum elementary medium (EMEM, Lonza) supplemented with 1 μg/ml trypsin (Roche diagnostics) and further incubated at 34 °C. Harvested supernatants were centrifuged at 1500 g for 10 min and stored at −70 °C until analysis. End point-titration assays were performed on confluent layers of MDCK cells in 96-well plates. Briefly, 50 μl of 10-fold serial dilutions of each virus was inoculated into four replicate wells. The 96-well microplates were incubated at 34 °C and the presence of cytopathic effects (CPE) monitored 3 days later under a microscope. The presence of virus in supernatants was also confirmed by hemagglutination tests using guinea pig erythrocytes. The TCID50 per ml values were determined using the Reed and Muench statistical method, as previously described (Moulès et al., 2011).

Electron microscopy

For ultrastructural investigations, mock- and infected cell cultures were fixed with 2% glutaraldehyde (Sigma) in 0.1 M sodium cacodylate (pH 7.3) buffer at room temperature for 30 min. After washing three times in 0.2 M sodium cacodylate buffer, cell cultures were post-fixed with 2% aqueous osmium tetroxide (EMS) and deshydrated in a graded series of ethanol at room temperature and embedded in Epon. After polymerization, ultrathin sections were collected on 300 mesh grids coated with formvar and stained with aqueous 1% uranyl acetate and lead citrate (Leïca Ultrostainer) before observations on a Philips CM 120 transmission electron microscope at an acceleration voltage of 80 kV.

For immunolabeling, cell monolayers were fixed 1 hour at room temperature with 2.5% paraformaldehyde (Sigma) in phosphate buffer 0.1 M (pH 7.2). After fixation, cells were scraped and pelleted for 15 min at 1500 rpm. After being washed two times for 15 min in 0.2 M phosphate buffer and centrifuged, cells were embedded in 2% agar, dehydrated in increasing concentrations of ethanol by progressive lowering of temperature (PLT), and finally embedded in Lowicryl K4M with a Leïca AFS. After polymerization, ultrathin sections were collected on nickel 300 mesh grids previously coated with formvar. In order to characterize the structures containing viral proteins, grids bearing Lowicryl sections were saturated during 1 hour with 1% bovine serum albumin (BSA) in 0.05 M TRIS/HCl pH 7.4 buffer, prior to incubation at 4 °C with primary rabbit polyclonal anti-NS1 (kindly provided by Dr. Juan Ortin) or goat polyclonal anti-M1 (PA1-85626, Thermo-scientific) in 1%BSA-TRIS/HCl 0.05 M pH 7.4.

After washing three times in TRIS/HCL (pH 7.4) and two times in TRIS/HCL (pH 8.2), the grids were incubated at room temperature (45 min) with goat anti-mouse antibodies (1:80) conjugated to gold particles (10 nm diameter, BB international). After washing with TRIS/HCl (pH 8.2) and TRIS/HCl (pH 7.4), grids were fixed in 4% glutaraldehyde and contrasted with 5% uranyl acetate in 50% ethanol prior to observation with a JEOL JEM-1400 electron microscope. To ensure the specificity of secondary antibodies, we

verified that no labeling occurred without prior primary antibody incubation.

EM experiments were performed in duplicate, three grids were observed for each conditions of infection or tranfection. Each observation was performed on at least 10 individual cells. All A549 and CEF cells displaying morphological signs and immunostaining of infection were considered, imaged and respective representative patterns were reported in the figures.

Immunofluorescence

A549 cells were fixed with 4% formaldehyde for 30 min and then permeabilized with 0.1% Triton X-100 in PBS (PBST) for 15 min at 4 °C. Mouse monoclonal anti-NP (17C2; kindly provided by Dr. Olivier Ferraris) or anti-M1 (AbCam, ab22396) and rabbit polyclonal anti-NS1 (gift from Dr. Juan Ortin) were used in PBST. After 1 h incubation at room temperature, the cover slips were washed in PBST and then incubated 30 min with goat anti-mouse and anti-rabbit Alexa Fluor 633-labeled or 488-labeled (Molecular Probes, Invitrogen), at concentrations recommended by the suppliers. Nuclei were counterstained with DNA-binding fluorochrome 4,6-diamidino-2-phenylindole (DAPI, Invitrogen). After washing with PBS, the cover slips were mounted with Fluoromount G (Cliniscience) and analyzed using a TCS SP2 confocal laser scanning microscope (Leica). Each observation was performed on at least 20 individual cells from 5 different large fields of view. For all observations, each representative pattern was reported.

Transfection and western blot

Transfection of plasmids into cells was performed using Lipofectamine 2000 (Invitrogen). According to the manufacturer's instructions 3 mg of pHW2000 plasmids were added to 10^6 cells for 48 hours. The efficiency of transfection was monitored using control plasmid coding for eGFP protein.

The level of expression of viral proteins was assessed by western blot. Proteins were extracted by scraping and syringing cells in 1X NuPAGE LDS buffer (Invitrogen). Fifteen to thirty micrograms of protein extract was separated on pre-cast 10% NuPAGE gels (Invitrogen). Monoclonal mouse anti-NP (C87050M, Meridian life science), anti-M1 (AbCam, ab22396) and goat polyclonal anti-NS1 (Santa cruz, Sc-17601) were used. Rabbit polyclonal Actin (Epitomics # S2613) was used as loading control.

Reverse genetics

H3N2 (MO), H3N2 delNS1, H5N2 (FI) and reassortant FINS, FIM and FIMNS viruses were generated by reverse genetics as previously described (Hoffman et al., 2000). Briefly, viral RNA was extracted by using QIAmp viral RNA minikit (Qiagen) from A/Moscow/10/99 and A/Panama/2007/99H3N2 and A/Finch/England/2051/94H5N2 infected MDCK cell culture supernatant, according to the manufacturer's instructions. Two-step RT-PCR was carried out for full-length amplification of each viral RNA gene segment from each virus, by using influenza A universal RT primers (Uni-12primer, Eurogentec, Belgium) as previously described (Moulès et al., 2011). The cDNA obtained from different genes were cloned into the pHW2000 vector (Hoffman et al., 2000). The pHW2000-delNS1 construct was generated by reverse transcription from NEP-mRNA using an oligo-dT primer followed by amplification via PCR using specific primers (5′ TAT TCG TCT CAG GGA GCA AAA GCA GGG TG-′3 and 5′ ATA TCG TCT CTT ATT AGT AGA AAC AAG GGT GTT TTT TAT TAA ATA AGC TGA AAT G-′3). Ligation of the PCR product into the pHW2000 plasmid resulted in the pHW2000-delNS1 construct that encodes only the NEP open reading frame flanked by the non-coding regions of the viral NS segment.

Recombinant virus generation was performed by transfection of 293T using sets of eight-plasmid pHW2000 systems, as previously described (Moulès et al., 2011). At 48 h, the culture supernatant containing the viruses was harvested and diluted at 1/10 in EMEM medium supplemented with TPCK-trypsin (1 μg/ml) to infect confluent layers of MDCK cells. After three passages on MDCK cells, titers were measured using standard methods. The delNS1 virus was amplified in 6 day-old-embryonated chicken eggs for three days. Each full genome of recombinant viruses was validated by sequencing.

Acknowledgments

We are grateful to Juan Ortin (CSIC, Madrid), Daniel Marc (INRA, Tours) and Romain Volmer (INRA, Toulouse) for helpful discussions and Xingyi Ge (Institut Pasteur), Linda Feghoul, Laurence Josset, Olivier Ferraris (VirPath), Andrea Zoehner (RKI), Denis Ressnikoff (Centre Commun de Quantimétrie, Lyon) and Elisabeth Erazzuriz (Centre Commun d'Imagerie Laennec, Université Lyon 1) for their technical assistance.

Appendix A. Supporting information

Supplementary data associated with this article can be found in the online version at http://dx.doi.org/10.1016/j.virol.2012.05.019.

References

Amorim, M.J., Digard, P., 2006. Influenza A virus and the cell nucleus. Vaccine 24 (44–46) 6651–6655.
Andersen, J.S., Lam, Y.W., Leung, A.K., Ong, S.E., Lyon, C.E., Lamond, A.I., Mann, M., 2005. Nucleolar proteome dynamics. Nature 433 (7021), 77–83.
Anisimova, E., Ghendon, Y., Markushin, S., 1980. Ultrastructural changes in cells induced by temperature-sensitive mutants of fowl plague virus at permissive and non-permissive temperature. J. Gen. Virol. 47 (1), 11–18, PubMed PMID:7365459.
Anisimová, Tučková, E., Vonka, V., Závadová, H., 1977. Ultrastructural changes induced by influenza viruses in permissive and nonpermissive cells. Virology 77 (1), 330–336.
Ayllon, J., Hale, B.G., Garcia-Sastre, A., 2012. Strain-specific contribution of NS1-activated PI3K signaling to influenza A virus replication and virulence. J. Virol. Feb 15.
Boulo, S., Akarsu, H., Ruigrok, R.W., Baudin, F., 2007. Nuclear traffic of influenza virus proteins and ribonucleoprotein complexes. Virus Res. 124 (1–2), 12–21.
Chan, J.K., Park, P.C., De Boni, U., 2000. Association of DNAse sensitive chromatin domains with the nuclear periphery in 3T3 cells *in vitro*. Biochem. Cell Biol. 78 (2), 67–78.
Ciampor, F., 1972. Electron microscopy of tissue culture cells infected with myxoviruses. I. Nucleo-cytoplasmic changes in A0-WSN influenza virus-infected chick embryo cells. Acta Virol. 16 (1), 9–16, PubMed PMID: 4110514.
Compans, R.W., Dimmock, N.J., 1969. An electron microscopic study of single-cycle infection of chick embryo fibroblasts by influenza virus. Virology 39 (3), 499–515.
Emmott, E., Wise, H., Loucaides, E.M., Matthews, D.A., Digard, P., Hiscox, J.A., 2010. Quantitative proteomics using SILAC coupled to LC-MS/MS reveals changes in the nucleolar proteome in influenza A virus-infected cells. J. Proteome Res. 9 (10), 5335–5345.
Fournier, E., Moules, V., Essere, B., Paillart, J.C., Sirbat, J.D., Isel, C., Cavalier, A., Rolland, J.P., Thomas, D., Lina, B., Marquet, R., 2012. A supramolecular assembly formed by influenza A virus genomic RNA segments. Nucleic Acids Res. 40 (5), 2197–2209.
Garcia-Sastre, A., Egorov, A., Matassov, D., Brandt, S., Levy, D.E., Durbin, J.E., Palese, P., Muster, T., 1998. Influenza A virus lacking the NS1 gene replicates in interferon-deficient systems. Virology 252 (2), 324–330.
Goic, B., Bustamante, J., Miquel, A., Alvarez, M., Vera, M.I., Valenzuela, P.D., Burzio, L.O., 2008. The nucleoprotein and the viral RNA of infectious salmon anemia virus (ISAV) are localized in the nucleolus of infected cells. Virology 379 (1), 55–63.
Goldsmith, C.S., Metcalfe, M.G., Rollin, D.C., Shieh, W.J., paddock, C.D., xu, X., Zaki, S.R., 2011. Ultrastructural characterization of pandemic (H1N1) 2009 virus. Emerg. Infect. Dis. 17 (11), 2056–2059.

Gomez-Puertas, P., Albo, C., Perez-Pastrana, E., Vivo, A., Portela, A., 2000. Influenza virus matrix protein is the major driving force in virus budding. J. Virol. 74 (24), 11538–11547.
Greco, A., 2009. Involvement of the nucleolus in replication of human viruses. Rev. Med. Virol. 19 (4), 201–214.
Hale, B.G., Randall, R.E., Ortin, J., Jackson, D., 2008. The multifunctional NS1 protein of influenza A viruses. J. Gen. Virol. 89 (Pt 10), 2359–2376.
Hiscox, J.A., 2007. RNA viruses: hijacking the dynamic nucleolus. Nat. Rev. Microbiol. 5 (2), 119–127, Review. PubMed PMID: 17224921.
Hiscox, J.A., 2006. Viruses and the Nucleus. Wiley LTD.
Hoffmann, E., Neumann, G., Kawaoka, Y., Hobom, G., Webster, R.G., 2000. A DNA transfection system for generation of influenza A virus from eight plasmids. Proc. Natl Acad. Sci. U. S. A. 97 (11), 6108–6113.
Huang, X., Liu, T., Muller, J., Levandowski, R.A., Ye, Z., 2001. Effect of influenza virus matrix protein and viral RNA on ribonucleoprotein formation and nuclear export. Virology 287 (2), 405–416.
Hui, E.K., Barman, S., Yang, T.Y., Nayak, D.P., 2003. Basic residues of the helix six domain of influenza virus M1 involved in nuclear translocation of M1 can be replaced by PTAP and YPDL late assembly domain motifs. J Virol. 77 (12), 7078–7092, Retraction in: Hui, E.K., Barman, S., Yang, T.Y., Tang, D.H., France, B., Nayak, D.P., 2006. J. Virol. 80 (20), 10289.
Jackson, S., Van Hoeven, N., Chen, L.M., Maines, T.R., Cox, N.J., Katz, J.M., Donis, R.O., 2009. Reassortment between avian H5N1 and human H3N2 influenza viruses in ferrets: a public health risk assessment. J. Virol. 83 (16), 8131–8140.
Josset, L., Frobert, E., Rosa-Calatrava, M., 2008. Influenza A replication and host nuclear compartments: many changes and many questions. J. Clin Virol. 43 (4), 381–390.
Josset, L., Textoris, J., Loriod, B., Ferraris, O., Moules, V., Lina, B., N'guyen, C., Diaz, J.J., Rosa-Calatrava, M., 2010. Gene expression signature-based screening identifies new broadly effective influenza a antivirals. PLoS One, 5 (10).
Karlas, A., Machuy, N., Shin, Y., Pleissner, K.P., Artarini, A., Heuer, D., Becker, D., Khalil, H., Ogilvie, L.A., Hess, S., M√§urer, A.P., Muller, E., Wolff, T., Rudel, T., Meyer, T.F., 2010. Genome-wide RNAi screen identifies human host factors crucial for influenza virus replication. Nature 463 (7282), 813–817.
Kash, J.C., Goodman, A.G., Korth, M.J., Katze, M.G., 2006. Hijacking of the host-cell response and translational control during influenza virus infection. Virus Res. 119, 111–120.
Keiner, B., Maenz, B., Wagner, R., Cattoli, G., Capua, I., Klenk, H.D., 2010. Intracellular distribution of NS1 correlates with the infectivity and interferon antagonism of an avian influenza virus (H7N1). J. Virol. 84 (22), 11858–11865.
König, R., Stertz, S., Zhou, Y., Inoue, A., Hoffmann, H.H., Bhattacharyya, S., Alamares, J.G., Tscherne, D.M., Ortigoza, M.B., Liang, Y., Gao, Q., Andrews, S.E., Bandyopadhyay, S., De Jesus, P., Tu, B.P., Pache, L., Shih, C., Orth, A., Bonamy, G., Miraglia, L., Ideker, T., García-Sastre, A., Young, J.A., Palese, P., Shaw, M.L., Chanda, S.K., 2010. Human host factors required for influenza virus replication. Nature 463 (7282), 813–817.
Kopp, J.V., Kempf, J.E., Kroeger, A.V., 1968. Cytoplasmic inclusions observed by electron microscopy late in influenza virus infection of chicken embryo fibroblasts. Virology 36 (4), 681–683, PubMed PMID: 5723676.
Krug, R.M., Yuan, W., Noah, D.L., Latham, A.G., 2003. Intracellular warfare between human influenza viruses and human cells: the roles of the viral NS1 protein. Virology 309 (2), 181–189.
Lamond, A.I., Sleeman, J.E., 2003. Nuclear substructure and dynamics. Curr. Biol. 13 (21), R825–R828.
Li, C., Hatta, M., Watanabe, S., Neumann, G., Kawaoka, Y., 2008. Compatibility among polymerase subunit proteins is a restricting factor in reassortment between equine H7N7 and human H3N2 influenza viruses. J Virol 82 (23), 11880–11888.
Liu, T., Ye, Z., 2004. Introduction of a temperature-sensitive phenotype into influenza A/WSN/33 virus by altering the basic amino acid domain of influenza virus matrix protein. J. Virol. 78 (18), 9585–9591.
Melen, K., Kinnunen, L., Fagerlund, R., Ikonen, N., Twu, K.Y., Krug, R.M., Julkunen, I., 2007. Nuclear and nucleolar targeting of influenza A virus NS1 protein: striking differences between different virus subtypes. J. Virol. 81 (11), 5995–6006.
Michaelis, M., Doerr, H.W., Cinatl Jr., J., 2009. An influenza A H1N1 virus revival—pandemic H1N1/09 virus. Infection 37 (5), 381–389.
Morrongiello, M.P., Dales, S., 1977. Characterization of cytoplasmic inclusions formed during influenza/WSN virus infection of chick embryo fibroblast cells. Intervirology 8 (5), 281–293.
Moulès, V., Terrier, O., Yver, M., Riteau, B., Moriscot, C., Ferraris, O., Julien, T., Giudice, E., Rolland, J.P., Erny, A., Bouscambert-Duchamp, M., Frobert, E., Rosa-Calatrava, B., Pu Lin, Y., Hay, A., Thomas, D., Schoehn, G., Lina, B., 2011. Importance of viral genomic composition in modulating glycoprotein content on the surface of influenza virus particles. Virology 414 (1), 51–62.
Munday, D.C., Hiscox, J.A., Barr, J.N., 2010. Quantitative proteomic analysis of A549 cells infected with human respiratory syncytial virus subgroup B using SILAC coupled to LC-MS/MS. Proteomics 10 (23), 4320–4334.
Murayama, R., Harada, Y., Shibata, T., Kuroda, K., Hayakawa, S., Shimizu, K., Tanaka, T., 2007. Influenza A virus non-structural protein 1 (NS1) interacts with cellular multifunctional protein nucleolin during infection. Biochem Biophys Res Commun 362 (4), 880–885.
Nagata, K., Kawaguchi, A., Naito, T., 2008. Host factors for replication and transcription of the influenza virus genome. Rev Med Virol 18 (4), 247–260.
Mayer, D., Molawi, K., Martínez-Sobrido, L., Ghanem, A., Thomas, S., Baginsky, S., Grossmann, J., García-Sastre, A., Schwemmle, M., 2007. Identification of cellular interaction partners of the influenza virus ribonucleoprotein complex and polymerase complex using proteomic-based approaches. J. Proteome Res. 6 (2), 672–682, Nature 2010 463 (7282) 818–822.
Naffakh, N., Tomoiu, A., Rameix-Welti, M.-A., van der Werf, S., 2008. Host restriction of avian influenza viruses at the level of the ribonucleoproteins. Annu. Rev. Microbiol. 62, 403–424.
Neumann, G., Noda, T., Kawaoka, Y., 2009. Emergence and pandemic potential of swine-origin H1N1 influenza virus. Nature 459 (7249), 931–939.
Neumann, G., Brownlee, G.G., Fodor, E., Kawaoka, Y., 2004. Orthomyxovirus replication, transcription, and polyadenylation. Curr. Top. Microbiol. Immunol. 283, 121–143.
Ozawa, M., Fujii, K., Muramoto, Y., Yamada, S., Yamayoshi, S., Takada, A., Goto, H., Horimoto, T., Kawaoka, Y., 2007. Contributions of two nuclear localization signals of influenza A virus nucleoprotein to viral replication. J. Virol. 81 (1), 30–41, Jan.
Palese, P., Shaw, M.L., 2007. Orthomyxoviridae: the viruses and their. replication. In: Fields, B.N., et al. (Eds.), Fields Virology, 5th ed , pp. 1647–1689.
Ruigrok, R.W., Barge, A., Durrer, P., Brunner, J., Ma, K., Whittaker, G.R., 2000. Membrane interaction of influenza virus M1 protein. Virology 15, 267 (2), 289–298.
Saito, Y., Yoshioka, I., Igarashi, Y., Nakagawa, S., 1970. Nuclear inclusions observed by electron microscope in Cynomolgus monkey kidney cells infected with influenza virus. Virology 40 (2), 408–410.
Shaw, M.W., Compans, R.W., 1978. Isolation and characterization of cytoplasmic inclusions from influenza A virus-infected cells. J Virol. 25 (2), 608–615.
Soubies, S.M., Volmer, C., Croville, G., Loupias, J., Peralta, B., Costes, P., Lacroux, C., Guérin, J.L., Volmer, R., 2010. Species-specific contribution of the four C-terminal amino acids of influenza A virus NS1 protein to virulence. J. Virol. 84 (13), 6733–6747.
Visintin, R., Amon, A., 2000. The nucleolus: the magician's hat for cell cycle tricks. Curr. Opin. Cell Biol. 12 (3), 372–377.
Volmer, R., Mazel-Sanchez, B., Volmer, C., Soubies, S.M., Guérin, J.L., 2010. Nucleolar localization of influenza A NS1: striking differences between mammalian and avian cells. Virol. J. 7, 63.
Watanabe, K., Fuse, T., Asano, I., Tsukahara, F., Maru, Y., Nagata, K., Kitazato, K., Kobayashi, N., 2006. Identification of Hsc70 as an influenza virus matrix protein (M1) binding factor involved in the virus life cycle. FEBS Lett. 580 (24), 5785–5790.
Wolff, T., Ludwig, S., 2009. Influenza viruses control the vertebrate type I interferon system: factors, mechanisms, and consequences. J. Interferon Cytokine Res. 29 (9), 549–557.
Yamanaka, K., Ishihama, A., Nagata, K., 1990. Reconstitution of influenza virus RNA-nucleoprotein complexes structurally resembling native viral ribonucleoprotein cores. J. Biol. Chem. 265 (19), 11151–11155.
Yoshida, T., Shaw, M.W., Young, J.F., Compans, R.W., 1981. Characterization of the RNA associated with influenza A cytoplasmic inclusions and the interaction of NS1 protein with RNA. Virology 110 (1), 87–97.
Zielecki, F., Semmler, I., Kalthoff, D., Voss, D., Mauel, S., Gruber, A.D., Beer, M., Wolff, T., 2010. Virulence determinants of avian H5N1 influenza A virus in mammalian and avian hosts: role of the C-terminal ESEV motif in the viral NS1 protein. J. Virol. 84 (20), 10708–10718.
Zimber, A., Nguyen, Q.D., Gespach, C., 2004. Nuclear bodies and compartments: functional roles and cellular signalling in health and disease. Cell Signal 16 (October 10), 1085–1104.
Zohari, S., Munir, M., Metreveli, G., Belàk, S., Berg, M., 2010. Differences in the ability to suppress interferon B production between allele A and allele B NS1 proteins from H10 influenza A viruses. Virol. J. 7 (1), 376.